PCCP

PAPER

Published on 14 January 2019
Licence and permissions

Cite this: *Phys. Chem. Chem. Phys.*, 2019, **21**, 2727

Stationary polaron properties in organic crystalline semiconductors

Marcelo Lopes Pereira Junior,[a] Rafael Timóteo de Sousa Júnior,[b] Geraldo Magela e Silva[a] and Luiz Antônio Ribeiro Júnior *[ac]

Received 7th November 2018,
Accepted 14th January 2019

DOI: 10.1039/c8cp06915h

rsc.li/pccp

Polarons play a crucial role in the charge transport mechanism when it comes to organic molecular crystals. The features of their underlying properties – mostly the ones that directly impact the yield of the net charge mobility – are still not completely understood. Here, a two-dimensional Holstein–Peierls model is employed to numerically describe the stationary polaron properties in organic semiconductors at a molecular scale. Our computational protocol yields model parameters that accurately characterize the formation and stability of polarons in ordered and disordered oligoacene-like crystals. The results show that the interplay between the intramolecular (Holstein) and intermolecular (Peierls) electron–lattice interactions critically impacts the polaron stability. Such an interplay can produce four distinct quasi-particle solutions: free-like electrons, metastable polarons, and small and large polarons. The latter governs the charge transport in organic crystalline semiconductors. Regarding disordered lattices, the model takes into account two modes of static disorder. Interestingly, the results show that intramolecular disorder is always unfavorable to the formation of polarons whereas intermolecular disorder may favor the polaron generation in regimes below a threshold for the electronic transfer integral strength.

1 Introduction

Organic semiconductors are one of the most promising materials for developing a new class of green energy solutions with good cost-efficiency compromise.[1] Their applications can range from active layers in commercial devices, such as the mature OLED technology,[2] to biocompatible electronics.[3] Behind the working principle of these applications, the formation and stability of charge carriers are fundamental steps to be considered towards the improvement of the devices' operation.[4,5]

It is well known that organic crystalline semiconductors exhibit two distinct types of electron–lattice interactions: local intramolecular (Holstein-type) and non-local intermolecular (Peierls-type).[6] The former denotes the carbon–carbon covalent bonds and the latter considers the weak van der Waals interactions.[7] For accurately describe such a class of material, the Holstein and Peierls approaches should merge at just one methodology named, henceforth, the Holstein–Peierls model.[8] This combined approach leads to the polaron concept in molecular crystals.[9] Polarons are formed by injecting (removing) an electron to (from) an unsaturated organic system inducing, consequently, deformations in the lattice. The interaction between the electron and lattice distortions leads to a configuration in which the carrier is spatially localized and coupled to a cloud of phonons. It is necessary to preserve such a mutual interplay to fulfill the presence of stable polarons, which govern the charge transport mechanism in organic molecular crystals.

Recently, the Holstein–Peierls model has been successfully used to study, mostly, the dynamical properties of polarons in organic molecular crystals.[10–15] Nevertheless, the role played by crystal's properties such as anisotropy, disorder degrees, and electron–phonon interactions on the polaron formation and, consequently, its stability remains poorly investigated. Furthermore, several relevant studies have focused only on understanding the impact of the molecular parameters on the charge mobility properties.[16–21]

In this work, by using a semi-classical Holstein–Peierls model, the formation and stability of polarons at organic semiconductors are investigated at a molecular scale. In the context of a two-dimensional tight-binding approach, a systematic numerical study is performed to understand the interdependence between the intra and intermolecular parameters of a model Hamiltonian, and its impact on the underlying properties of polarons in isotropic and anisotropic oligoacene-like crystals, such as pentacene[22] and rubrene.[23] Our computational protocol also considers the influence of disordered lattices on the polaron formation mechanism.

[a] *Institute of Physics, University of Brasília, Brasília, 70910-900, Brasília, Brazil*
[b] *Department of Electrical Engineering, University of Brasília, CP04455, Brasília, 70919-970, Brazil*
[c] *Department of Physics, Chemistry and Biology (IFM), Linköping University, SE-581 83 Linköping, Sweden. E-mail: luiju@ifm.liu.se*

2 Methodology

The model Hamiltonian adopted here considers both intramolecular (Holstein-type)[24,25] and intermolecular (Peierls-type)[26] electron–lattice (e–l) interactions for a two-dimensional array of molecules in the presence of periodic boundary conditions. In this model, a (i,j) site denotes a molecule that possesses three degrees of freedom: one internal (intramolecular) vibrational mode $u_{i,j}$ and two external (intermolecular) vibrational modes v_i^x and v_i^y, which describe the motion of a molecule in the x- and y-directions, respectively. It is worthwhile to mention that most organic crystalline semiconductors present strong in-plane electronic interactions and substantially weaker out-plane ones, which leads, consequently, to an in-plane localization of the charge carriers. Hence, a two-dimensional lattice of molecules is used to describe the essential physics behind the polaron properties in these materials.

According to the representation of Fig. 1, our model Hamiltonian assumes the form $\hat{H} = \hat{H}_1 + \hat{H}_2$, where H_1 and H_2 denote the intra and intermolecular contributions as in the following:

$$\hat{H}_1 = \sum_{i,j} \left(\varepsilon_{i,j} + \alpha_1 u_{i,j}\right) \hat{c}_{i,j}^{\dagger} \hat{c}_{i,j} \tag{1}$$

and

$$\begin{aligned} \hat{H}_2 \;=\; & \sum_{i,j} \left(J^x_{i+1,j,i,j} \hat{c}_{i,j}^{\dagger} \hat{c}_{i+1,j} + \text{h.c.} \right) \\ & + \sum_{i,j} \left(J^y_{i,j+1,i,j} \hat{c}_{i,j+1}^{\dagger} \hat{c}_{i,j} + \text{h.c.} \right). \end{aligned} \tag{2}$$

In eqn (1), α_1 represents the intramolecular e–l coupling strength and $\varepsilon_{i,j}$ the site eigenenergies. In a completely ordered system, all eigenenergies are identical. The intermolecular e–l interactions, in turn, are included in our model by means of the intermolecular transfer integrals, $J^x_{i+1,j,i,j}$ and $J^y_{i,j+1,i,j}$, in the x- and y-directions, respectively, which are written in the form

$$J^x_{i+1,j,i,j} = J^x_0 - \alpha^x_2 (v^x_{i+1,j} - v^x_{i,j}) \tag{3}$$

and

$$J^y_{i,j+1,i,j} = J^y_0 - \alpha^y_2 (v^y_{i,j+1} - v^y_{i,j}). \tag{4}$$

In the equations above, $\alpha_2^{x,y}$ denotes the intermolecular e–l coupling strength and $J_0^{x,y}$ is the strength of the transfer integral in a system where the molecules are equally spaced. The operator $\hat{c}^{\dagger}_{i,j}(\hat{c}_{i,j})$ creates (annihilates) an electron at the (i,j)-th site of the lattice.

Disorder inevitably exists in the molecular crystals. It can appear in terms of intermolecular vibrational modes that, to first order, affect the intermolecular interactions, that is, J^x and J^y, and in terms of static defects such as crystal imperfections and the presence of impurities, that is introduced in our study by means of $\varepsilon_{i,j}$. We have introduced perturbations in the electronic degree of freedom by using two different parameters that can play the role of changing the intra and intermolecular energy quantities in a distinct fashion. Both energetic parameters could indirectly impact the physical disorder in the crystals structure (see eqn (3) and (4)) since our model includes both the intra and intermolecular electron–lattice coupling parameters.

The potential energy V of the system (lattice contribution) considers distinct harmonic oscillators, the intra and intermolecular vibrational modes:

$$\begin{aligned} V = & \frac{1}{2} K_1 \sum_{i,j} \left(u_{i,j}\right)^2 \\ & + \frac{1}{2} K_2 \sum_{i,j} \left[\left(v^x_{i+1,j} - v^x_{i,j} \right)^2 + \left(v^y_{i,j+1} - v^y_{i,j} \right)^2 \right]. \end{aligned} \tag{5}$$

In this equation, K_1 and K_2 refer to the intra and intermolecular force constants, respectively.

The total energy of the system includes both the electronic and lattice degrees of freedom and has the form

$$E_{\text{tot}} = \Psi \hat{H}_{\text{elec}} \Psi + V, \tag{6}$$

where the electronic wavefunction Ψ comes from the solution of the time-independent Schrödinger equation:

$$\hat{H}_{\text{elec}} \Psi = E_{\text{elec}} \Psi. \tag{7}$$

The ground state geometries for a given set of parameters derive from energy optimized structures by employing the Resilient backPROPogation algorithm (RPROP).[27] This algorithm is used to solve self-consistently the equations presented above. In order to do so, we begin by constructing $\hat{H}_{\text{elec}}$ based in a arbitrary set of positions for $\{u\}$, $\{v^x\}$, and $\{v^y\}$. By solving the eqn (7), a new set of positions – that will serve as input for $\hat{H}_{\text{elec}}$ in a new iteration – is obtained. The derivatives of the total energy with respect to $u_{i,j}$, $v^x_{i,j}$, and $v^y_{i,j}$ follow directly from the expressions given above. Iterative repetitions of this procedure yield a self-consistent initial

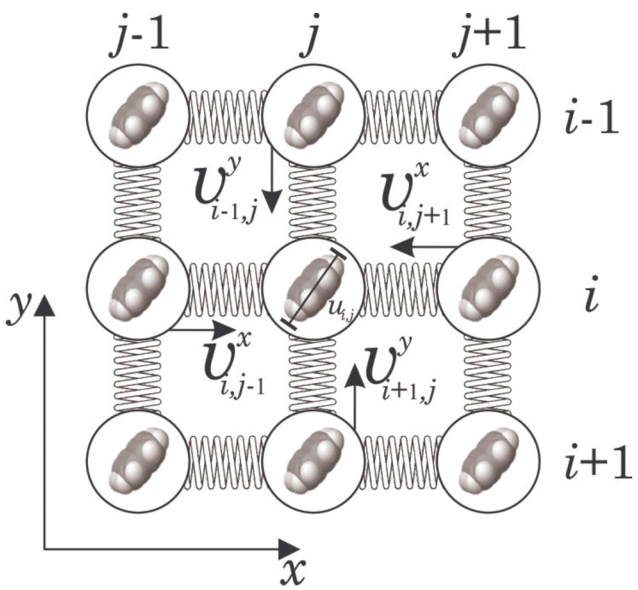

Fig. 1 Schematic representation of our model two-dimensional pentacene crystal. The index i (x-direction) denotes the "rows" whereas j (y-direction) labels the "columns". u_{ij} is the internal (intramolecular) vibrational mode and v_i^x and v_i^y are the two external (intermolecular) vibrational modes, which denote the motion of a molecule in the x- and y-directions, respectively.

state when the set of positions is close enough between successive iterations.

3 Results

In order to determine the regimes where stable polarons are formed and, consequently, to derive its underlying stationary properties, the ground state configurations for different parameter sets are obtained. The calculations are performed on a system of 20 × 20 sites, *i.e.*, 400 molecules. Our numerical protocol is based in determining the formation and stability of polarons in ordered and disordered oligoacene-like crystals, with particular interest on pentacene layers. In this way, the model parameters are settled as $J_0^{x,y}$ = 50 meV, K_1 = 14 eV Å^{-2} and K_2 = 0.9 eV Å^{-2} for the realizations where the impact of the interplay between the intra and intermolecular e–l interactions is taken into account. For these calculations, α_1 and α_2 range in the interval 0–2.5 eV Å^{-1}. In the cases where disordered lattices are studied, α_1 and α_2 are defined as 1.8 eV Å^{-1} and 0.4 eV Å^{-1}, respectively. Here, we have considered two different types of disorder: the intra and intermolecular ones, which are based in a randomly generated set of $\varepsilon_{i,j}$ and $J_{i,j}^{x,y}$, respectively. Importantly, the parameters used in the present work were derived from results of electronic structure calculations reported in the literature.[28–33] These calculations, in turn, were based in properties such as the lattice crystallographic arrangement and Raman spectroscopy data.

As mentioned in our recent work, a useful tool for characterizing the polaron stability is the inverse participation ratio (IPR) with respect to the charge density.[34–36] This quantity is a measure of how many sites share the charge. IPR values close to zero denotes systems in which the polaron is not stable and the quasi-particle solution, in this case, is a free-like electron. If the IPR lies in the range of 0.2–0.4, a metastable polaron solution is obtained. In this case, the molecular charge is equally distributed over a square of four molecules in isotropic systems (two-dimensional nature) or in two molecules of the same line in the molecular array for anisotropic lattices (one-dimensional nature). For IPR values between 0.4 and 0.8, the charge is usually shared by five molecules, considering both isotropic and anisotropic systems, and the resulting quasi-particle is named large polaron, following the Holstein terminology.[34] Large polarons are typical solutions in Holstein–Peierls systems, *i.e.*, when the interplay between local and non-local electron–lattice interactions are taken into account.[6] Moreover, this particular kind of charge carrier is the most useful for describing the charge transport mechanism in organic molecular crystals due to the nature of its charge localization. Finally, IPR values greater than 0.8 point to solutions in which the molecular charge is essentially localized in one molecule. This kind of structure is termed small polaron.[6]

With the details about our computational approach in mind, we can now turn to the discussions of the results. We first begin by analyzing the impact of the parameter space in forming the quasi-particles, obtained after optimizing the ground state geometries. Based on the discussions above about the IPR usefulness, Fig. 2 presents the impact of the interplay between the Holstein (intramolecular) and Peierls (intermolecular) parameters on the stability of polarons. It is worth to stress that in this case we are considering the case for ordered crystals ($\varepsilon_{i,j}$ = 0). In Fig. 2, panel (a) shows the nature of the charge carriers formed in isotropic systems with respect to the transfer integrals, *i.e.*, $J_0^x = J_0^y$ = 50 meV. Panel (b) considers a lattice with moderate degree of anisotropy (J_0^x = 50 meV and J_0^y = 25 meV). And panel (c) shows a highly anisotropic case (J_0^x = 50 meV and J_0^y = 0).

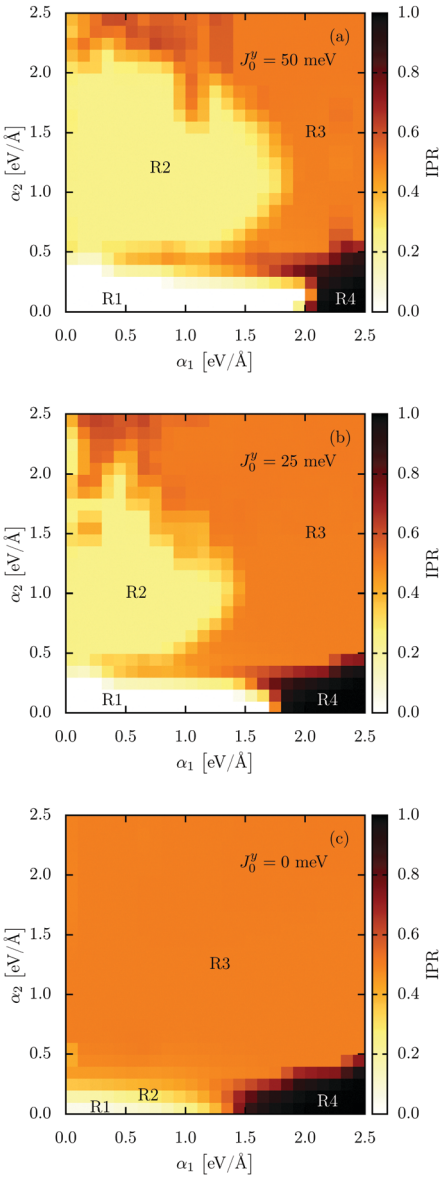

Fig. 2 The phase diagram for the formation of quasi-particles. The regions R1, R2, R3, and R4 within the panels depict the parameter space where ground state geometry calculations yield free-like electrons, metastable, large, and, small polarons, respectively. Here, panel (a) shows the nature of the charge carriers formed in isotropic systems regarding the transfer integral, *i.e.*, $J_0^x = J_0^y$ = 50 meV, panel (b) considers a lattice with moderated degree of anisotropy (J_0^x = 50 meV and J_0^y = 25 meV), and panel (c) shows a highly anisotropic case (J_0^x = 50 meV and J_0^y = 0).

These panels present a phase diagram divided into four distinct regions, each one denoting the range of values for the intra (α_1) and intermolecular (α_2) electron–lattice coupling strengths that yield a particular species of charge carrier. In all the panels, R1, R2, R3, and R4 denote the regions where ground state geometry calculations yield free-like electrons, metastable, large, and, small polarons, respectively. It is worthwhile to mention that our previous research[34] presents the ground state configuration regarding the lattice deformations and the molecular charge localization for a stable polaron. Moreover, we have showed that polarons in organic crystalline semiconductors are dynamically stable for electric field strengths smaller than 2.5 mV Å^{-1} or thermal baths smaller than 200 K.[34] For values of electric field and temperature above these critical regimes, the charge decouples from the local lattice deformations and the polaron dissociates spreading its charge through out the lattice.

In Fig. 2(a), the isotropic case, one can see that the dominant region is R2, where metastable polarons are dominating. Such a kind of charge carrier is termed metastable due to its two-dimensional nature for the charge localization and the lattice distortions, which resemble a large polaron, but it is not dynamically stable. Moreover, metastable polarons are dominant in isotropic systems, leading to a sharing configuration for the molecular charge in both directions depending on the interplay between α_1 and α_2. The second most common species of charge carrier found in our calculations, when it comes to isotropic systems, is the large polaron (region R3). Large polarons arise when the strength of intermolecular interactions, around the site with the additional charge, overcome the intramolecular e–l interactions of that particular lattice unit. As a consequence, the charge delocalizes over the neighboring sites at both directions. Even so, part of the molecular charge stays in a central unit and the rest is shared between four neighbors, as reported in ref. 34. In the R4 region, the reason for the strong charge localization is the difference between the α_1 and α_2 strengths. According to our calculations, small polarons arise when α_1 is almost five times higher than α_2. Such a kind of charge carrier is of less interest in the context of organic molecular crystals, mostly due to its two-dimensional nature presented in the field-induced charge transport mechanism.[6] The other species of quasi-particle obtained from our calculations is the free-like electron (region R1). Due to the weak intramolecular and intermolecular e–l interactions, the lattice do not trap the additional charge to form polarons. Since polarons play a dominant role in the charge transport mechanism below the mobility threshold, the parameter space that yields free-electrons is out of context.

The same type of phase diagram displayed in Fig. 2(a) is also obtained here for anisotropic systems, as depicted in Fig. 2(b and c). In Fig. 2(b), the strength of the transfer integral in the *x*-direction is 50 meV whereas in the *y*-direction it is settled as 25 meV. In this anisotropic system, the phase diagram shows a clear reduction for the domain of metastable polarons, R2 region, when compared to the isotropic case (see Fig. 2(a)). Moreover, the parameter spaces to generate free-electrons (region R1) and small polarons (region R4) have not suffered substantial changes. Conversely, the domain region denoting large polarons notably increases. It is important to mention that, in this case, the polaronic charge essentially lies in a line of the molecular array, *i.e.*, the formed charge carrier is still a large polaron. However, it assumes a quasi-one-dimensional nature. For the sake of completeness, we have also investigated the polaron stability in the limit of anisotropy, *i.e.*, $J_0^y = 0$, as depicted in Fig. 2(c). Since the electronic overlap between adjacent lines of the molecular array is turned off, the polaronic charge lies solely in one line, *i.e.*, the line that contains the extra electron. Moreover, we can also realize that the regions R1 and R2 almost disappear in this case. Due to the confinement of the charge in a particular line of molecules, even small strengths of α_2 can act to promote the charge localization by forming stable large polarons (see region R3 in Fig. 2(c)). We also note a small increase in the domain region (R4) of small polarons. It is possible to realize from Fig. 2 that anisotropy can favor the formation of small polarons, once the carrier tends to localize in one molecular line for smaller J_0^y.

Albeit organic molecular crystals can present a high degree of order, they present local defects in the lattice structure (disordered regions) after the layer fabrication.[23] Moreover, a detailed knowledge about the impact of the disorder degree on the stationary properties of polarons is not available and also difficult to control experimentally. Therefore, this study may enlighten the understanding of the underlying polaron properties in molecular crystals when the disorder is a dominant effect. It is well known that there are different static and dynamical ways in which the disorder can appear in these materials.[23] Here, we focus on two different modes for the static disorder: the on-site (intramolecular) and hopping (intermolecular) disorders. The random variables are $\varepsilon_{i,j}$, J_R^x and J_R^y, taken from a rectangular distribution of width W on the interval [0,1]. For the intermolecular disorder case, the random transfer integrals can reach values of $J_R^{x,y} = J_0^{x,y} \pm W$. To obtain a good insight about how the disorder can affect the stationary polaron properties, we have performed 20 000 realizations for five different strengths of W in each case. In this way, Fig. 3 and 4 show the impact of the lattice disorder degree on the polaron formation energy (E_P) and the lattice reorganization energy (λ), respectively. In Fig. 3(a) and 4(a), the transfer integral values are randomly generated and the center of the distribution is 50 meV. In these cases, we impose random configurations that can form nonlocal lattice distortions with or without the presence of an additional charge. Therefore, the lattice is said disordered. On the other hand, Fig. 3(b) and 4(b) present the cases where the disorder is imposed by randomly changing the on-site energies, keeping the transfer integral values for both directions fixed at 50 meV. This arrangement for the on-site energies also leads to the formation of nonlocal lattice distortions for both neutral and charged lattices. The polaron formation energy is the difference between the neutral ground state and relaxed conformation energies in the presence of an additional charge.[6] The total reorganization energy, in turn, accounts for the energy cost in displacing the lattice sites, from their equilibrium position, in the presence of an extra charge and can be calculated as $\lambda = \lambda_0/\mathrm{IPR}$, where λ_0 is the reorganization energy for the removal of a carrier from a single site.[37] In our calculations, λ_0 is 59 meV, according to ref. 23.

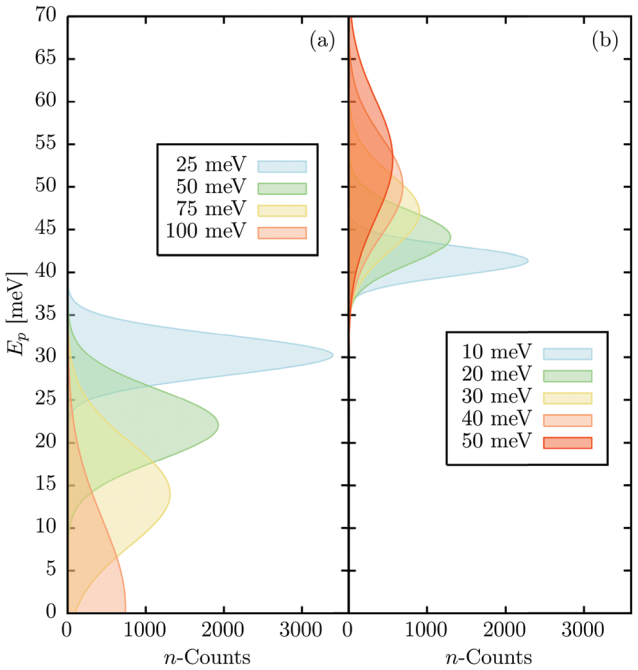

Fig. 3 Polaron formation energies E_P as a function of the number of counts (n-counts) for which the E_P is calculated after obtaining the ground state geometries for a given set of $\varepsilon_{i,j}$ or $J^{x,y}$, which are randomly generated. W_1 and W_2 are the reach of the rectangular distribution, on the interval [0,1], for the strength of the on-site energies (panel (a)) and transfer integrals (panel (b)), respectively.

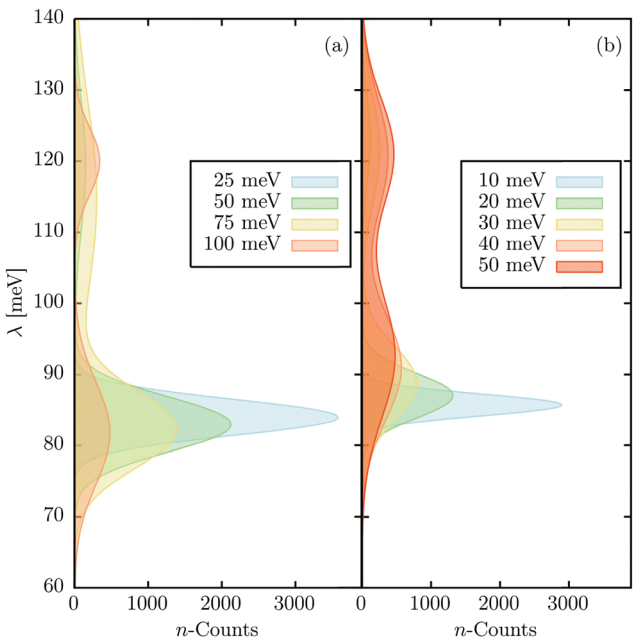

Fig. 4 Lattice reorganization energies λ as a function of the number of counts (n-counts) for which the λ is calculated after obtaining the ground state geometries for a given set of $\varepsilon_{i,j}$ or $J_0^{x,y}$, which are randomly generated. W_1 and W_2 are the reach of the rectangular distribution, on the interval [0,1], for the strength of the on-site energies (panel (a)) and transfer integrals (panel (b)), respectively.

Fig. 3 depicts the resulting polaron formation energies. In this figure, panels Fig 3(a) and (b) display the impact of the disorder degree on the polaron formation for the intra (W_1) and intermolecular channels (W_2), respectively. In this case, the transfer integrals in x- and y-directions are 50 meV. Note that all values obtained in the calculation of E_P lie in a realistic regime, since, in the context of semiconducting molecular crystals, E_P is in the order of 100 meV or less.[38] In Fig. 3(a) – where W_1 spans from 25 meV up to 100 meV – it can be seen that E_P follows an inverse relation with the strength of the on-site energies. It means that disorder is an unfavorable effect to form stable polarons. In the results presented in Fig. 3(a), E_P values in the interval [20,35] meV yield stable polarons. In this way, one can note from this figure that only the ground state calculations for W_1 = 25 meV yielded stable polarons in all realizations. The E_P average value in this case is approximately 30 meV. For W_1 values greater than this critical limit, the on-site energies on average are close to the strengths of the transfer integrals $J_0^{x,y}$. This trend breaks the suitable balance between charge localization and lattice deformations, which is necessary to form stable polarons. Again, an overview about the inter-dependence of ground state lattice geometries and molecular charge localization to yield stable polarons is in ref. 34. For the intra-chain disorder threshold simulated here, W_1 = 100 meV, one can realize that the average value of E_P is zero, as depicted in Fig. 3(a). This value for the on-site disorder is two times higher than the values adopted for the transfer integrals in x- and y-directions. Based on this result, we suggest $\varepsilon_{i,j} = 2 \times J_0^{x,y}$ as a critical limit to form stable polarons.

The intermolecular disorder oppositely tends to increase the E_P energies, as shown in Fig. 3(b). For the results presented in this figure, $\varepsilon_{i,j} = 0$. As previously mentioned, E_P is the potential energy difference between the neutral ground state and the relaxed state in the presence of an extra charge ($E_\pm$). For stable polarons, $E_P > 20$ meV and can be calculated as $E_P = 2(J_0^x + J_0^y) - E_\pm$.[6] From this equation, one can note that E_P is directly proportional to the strengths of the molecular transfer integral in both directions. Moreover, since an increase in the transfer integral rises the charge delocalization, the formation of stable polarons is favored in this particular disorder channel. However, we have obtained that there is a critical value for W_2, *i.e.*, 100 meV, where above it no polaron is formed due to the high degree of charge delocalization. In this regime of W_2, the molecular charge is not locally trapped, which substantially lowers the IPR value is a such a way that the system resembles a lattice containing a free-like electron.

It is important to stress that the reorganization energy obtained in our calculations for a lattice containing a stable polaron is about 90 meV, for isotropic and ordered systems. This value is in good agreement with the results in the relevant theoretical work.[38] As showed above, λ is derived from the IPR calculation that, in its turn, gives a measure of the charge localization in the lattice. The trends presented in Fig. 4(a and b) are qualitatively similar. However, there are basic differences between these two disorder types. Once the predominant effect of the intrachain disorder is of localizing the charge, the IPR

values for this case are, on average, higher and it ends by lowering the value of the lattice reorganization energy. The *n*-counts for the intrachain disorder (W_1) present, essentially, values for λ smaller than 90 meV, as shown in Fig. 4(a). Consistently, this fact suggests that systems that do no allow the formation of stable polarons, present small reorganization energy. The limit for this case is the energy required for the removal of a carrier from a single site, *i.e.*, λ_1. On the other hand, in the presence of an intermolecular disorder, we obtained that there is a trend of balance between *n*-counts of λ values below and above 100 meV, as can be inferred from Fig. 4(b). Since an increase in the strength of the intermolecular integrals leads, necessarily, to an increase in the molecular charge delocalization (taking into account the W_2 threshold mentioned above), the IPR values, in this case, tend to be low, which ends by lifting λ. Such an equilibrium in the λ distribution for high W_2 values does not take place in the case of intramolecular disorder. Moreover, it is worth to stress that, if the charge remains coupled to the lattice, the charge delocalization process increase the degree of lattice distortion due to the surrounding media polarization by the presence of charge. In this situation, more lattice sites are displaced from their equilibrium position. This process increases the lattice total energy, as can be seen from Fig. 4(b).

4 Conclusions

In summary, the stationary properties of polarons at organic semiconducting crystals are numerically investigated here by employing a two-dimensional Hamiltonian that considers two distinct degrees of freedom for the electron–lattice interactions: one local (Holstein-type) and one non-local (Peierls-type). The produced outcomes, after ground state calculations for different parameter sets, point to the formation of quasi-particles of distinct nature. Depending on the interplay between the intra and intermolecular electron–lattice interactions, free-like electrons, and metastable, small, and large polarons may be formed. The most common species of charge carrier yielded in our calculations, when it comes to both isotropic and anisotropic crystals, is the large polaron. The two-dimensional nature of the molecular charge delocalization combined with formation energy obtained for this charge carrier, around 30–90 meV, lies in realistic regimes. Furthermore, since large polarons play a dominant role in the charge transport mechanism below the mobility threshold, the parameter spaces to form free-electrons, metastable, or small polarons though determined are not of interest. The formation of stable polarons is also investigated in lattices containing disorder. Here, we consider two different types of a static disorder: an intramolecular (disorder for on-site energies) and an intermolecular (disorder for transfer integrals). In the former, the disorder inhibits the formation of polarons by promoting the increase in the localization of the charge in a single molecule whereas in the latter it can be a favorable effect by enhancing the charge localization in a region up to a certain critical limit where, above it, the charge delocalizes and the resulting structure resembles a free-like electron.

Conflicts of interest

There are no conflicts to declare.

Acknowledgements

The authors gratefully acknowledge the financial support from Brazilian Research Councils CNPq, CAPES, and FAP-DF and CENAPAD-SP for providing the computational facilities. This research work has the support of the Brazilian Ministry of Planning, Development and Management (Grants 005/2016 DIPLA – Planning and Management Directorate, and 11/2016 SEST – State-owned Federal Companies Secretariat) and the DPGU – Brazilian Union Public Defender (Grant 066/2016). L. A. R. J. and G. M. S. gratefully acknowledge the financial support from FAP-DF grants 0193.001.511/2017 and 0193.001766/2017, respectively. Finally, L. A. R. J. would like to thank Sven Stafström for valuable discussions.

Notes and references

1 Q. Zhang, W.-T. Wang, C.-Y. Chi, T. Wächter, J.-W. Chen, C.-Y. Tsai, Y.-C. Huang, M. Zharnikov, Y. Tai and D.-J. Liaw, *Energy Environ. Sci.*, 2018, **11**, 682–691.
2 C. Adachi, M. A. Baldo, M. E. Thompson and S. R. Forrest, *J. Appl. Phys.*, 2001, **90**, 5048.
3 S. Liu, Y. Fu, G. Li, L. Li, H. K. Law, X. Chen and F. Yan, *Adv. Mater.*, 2017, **29**, 1701733.
4 O. Ostroverkhova, *Chem. Rev.*, 2016, **117**, 13279–13412.
5 H. Oberhofer, K. Reuter and J. Blumberger, *Chem. Rev.*, 2017, **117**, 10319–10357.
6 S. Stafström, *Chem. Soc. Rev.*, 2010, **39**, 2484–2499.
7 A. Troisi, *Chem. Soc. Rev.*, 2011, **40**, 2347–2358.
8 A. Zhugayevych and S. Tretiak, *Annu. Rev. Phys. Chem.*, 2015, **66**, 305–330.
9 M. Hultell and S. Stafström, *Chem. Phys. Lett.*, 2006, **428**, 446–450.
10 M. Elham and S. Stafström, *J. Chem. Phys.*, 2013, **138**, 184104.
11 M. Elham and S. Stafström, *Phys. Lett. A*, 2012, **376**, 1807–1811.
12 A. Troisi and G. Orlandi, *Phys. Rev. Lett.*, 2006, **96**, 086601.
13 A. Troisi, D. L. Cheung and D. Andrienko, *Phys. Rev. Lett.*, 2009, **102**, 116602.
14 D. L. Cheung and A. Troisi, *Phys. Chem. Chem. Phys.*, 2008, **10**, 5941–5952.
15 J. Dong, W. Si and C.-Q. Wu, *J. Chem. Phys.*, 2016, **144**, 144905.
16 Z. Shuai, H. Geng, W. Xu, Y. Liao and J.-M. André, *Chem. Soc. Rev.*, 2014, **43**, 2662–2679.
17 Y. Olivier, V. Lemaur, J. L. Brédas and J. Cornil, *J. Phys. Chem. A*, 2006, **110**, 6356–6364.
18 Y. Li, Y. Yi, V. Coropceanu and J.-L. Brédas, *Phys. Rev. B: Condens. Matter Mater. Phys.*, 2012, **85**, 245201.
19 Y. Li, V. Coropceanu and J.-L. Brédas, *J. Chem. Phys.*, 2013, **138**, 204713.
20 V. Coropceanu, H. Li, P. Winget, L. Zhu and J.-L. Brédas, *Annu. Rev. Mater. Res.*, 2013, **43**, 63–87.
21 E. F. Valeev, V. Coropceanu, D. A. da Silva Filho, S. Salman and J.-L. Brédas, *J. Am. Chem. Soc.*, 2006, **128**, 9882–9886.

22 A. R. Murphy and J. M. J. Fréchet, *Chem. Rev.*, 2007, **107**, 1066–1096.
23 V. Coropceanu, J. Cornil, D. A. da Silva Filho, Y. Olivier, R. Silbey and J.-L. Brédas, *Chem. Rev.*, 2007, **107**, 926–952.
24 T. Holstein, *Ann. Phys.*, 1959, **8**, 325–342.
25 T. Holstein, *Ann. Phys.*, 1959, **8**, 343–389.
26 K. Hannewald, V. M. Stojanović, J. M. T. Schellekens, P. A. Bobberta, G. Kresse and J. Hafner, *Phys. Rev. B: Condens. Matter Mater. Phys.*, 2004, **69**, 075211.
27 M. Riedmiller and H. Braun, *Proceedings of the IEEE International Conference on Neural Networks*, 1993, vol. 1, pp. 586–591.
28 R. S. Sánchez-Carrera, P. Paramonov, G. M. Day, V. Coropceanu and J.-L. Brédas, *J. Am. Chem. Soc.*, 2010, **132**, 14437–14446.
29 R. S. Sánchez-Carrera, V. Coropceanu, D. A. da Silva Filho, R. Friedlein, W. Osikowicz, R. Murdey, C. Suess, W. R. Salaneck and J.-L. Brédas, *J. Phys. Chem. B*, 2006, **110**, 18904–18911.
30 A. Troisi and G. Orlandi, *J. Phys. Chem. A*, 2006, **110**, 4065–4070.
31 H. A. v. Laarhoven, J. Flipse, M. Koeberg, M. Bonn, E. Hendry, G. Orlandi, O. D. Jurchescu, T. T. M. Palstra and A. Troisi, *J. Chem. Phys.*, 2008, **129**, 044704.
32 V. Coropceanu, M. Malagoli, D. A. da Silva Filho, N. E. Gruhn, T. G. Bill and J. L. Brédas, *Phys. Rev. Lett.*, 2002, **89**, 275503.
33 J. L. Brédas, J. P. Calbert, D. A. da Silva Filho and J. Cornil, *Proc. Natl. Acad. Sci. U. S. A.*, 2002, **99**, 5804–5809.
34 L. A. R. Junior and S. Stafström, *Phys. Chem. Chem. Phys.*, 2015, **17**, 8973–8982.
35 L. A. R. Junior and S. Stafström, *Phys. Chem. Chem. Phys.*, 2016, **18**, 1386–1391.
36 L. A. R. Junior and S. Stafström, *Phys. Chem. Chem. Phys.*, 2017, **19**, 4078–4084.
37 R. P. Fornari, P. W. Blom and A. Troisi, *Phys. Rev. Lett.*, 2017, **118**, 086601.
38 N. E. Gruhn, D. A. da Silva Filho, T. G. Bill, M. Malagoli, V. Coropceanu, A. Kahn and J.-L. Brédas, *J. Am. Chem. Soc.*, 2002, **124**, 7918–7919.